

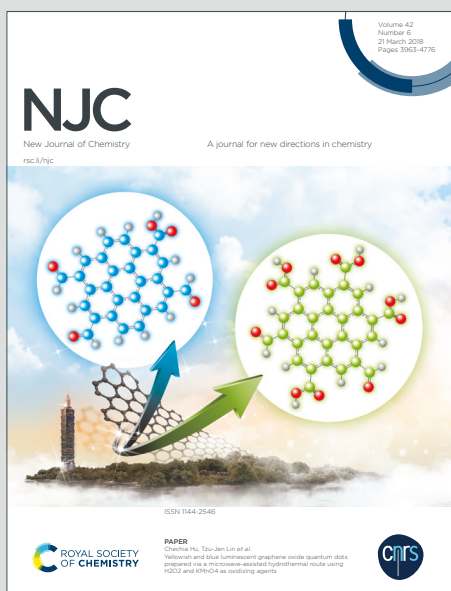
NJC

New Journal of Chemistry

Accepted Manuscript

A journal for new directions in chemistry

This article can be cited before page numbers have been issued, to do this please use: S. D. Naik, S. K. Apte, S. N. Garaje, Y. A. Sethi, M. D. Shinde, S. S. Arbuj, B. B. Kale and R. Sonawane, *New J. Chem.*, 2020, DOI: 10.1039/D0NJ01323D.



This is an Accepted Manuscript, which has been through the Royal Society of Chemistry peer review process and has been accepted for publication.

Accepted Manuscripts are published online shortly after acceptance, before technical editing, formatting and proof reading. Using this free service, authors can make their results available to the community, in citable form, before we publish the edited article. We will replace this Accepted Manuscript with the edited and formatted Advance Article as soon as it is available.

You can find more information about Accepted Manuscripts in the [Information for Authors](#).

Please note that technical editing may introduce minor changes to the text and/or graphics, which may alter content. The journal's standard [Terms & Conditions](#) and the [Ethical guidelines](#) still apply. In no event shall the Royal Society of Chemistry be held responsible for any errors or omissions in this Accepted Manuscript or any consequences arising from the use of any information it contains.

Journal Name

ARTICLE

Facile Template Free Approach for the Large Scale Solid Phase Synthesis of Nanocrystalline XIn_2S_4 ($X=Cd/Zn$) and its Photocatalytic Performance for H_2 Evolution.

Received 00th January 20xx,
Accepted 00th January 20xx

DOI: 10.1039/x0xx00000x

www.rsc.org/

Sonali D. Naik, Sanjay K. Apte,*^a Sunil N. Garaje, Yogesh A. Sethi, Manish D. Shinde, Sudhir A. Arbut, Bharat B. Kale and Ravindra S. Sonawane*^b

In the present study, we have **demonstrated a unique approach** for the synthesis of nanostructured **ternary metal sulphides**, XIn_2S_4 ($X = Cd, Zn$) by simple, template free and low temperature solid phase reaction. Stoichiometric amount of precursors such as CdO/ZnO , In_2O_3 and Thiourea were mixed homogeneously and heated at $150^\circ C$ for different time intervals to produce nanostructured XIn_2S_4 . The molar ratio of the precursors was varied and among the different ratios, the molar ratio 1:1:8 is found to be optimum for the growth of phase pure nano crystalline XIn_2S_4 . X-ray analysis confirms the formation of cubic spinel Cadmium Indium Sulfide ($CdIn_2S_4$) and hexagonal Zinc Indium Sulfide ($ZnIn_2S_4$). HRTEM analysis confirms the formation of nanostructures of XIn_2S_4 with spherical and rod like mixed morphology. The band gap of as synthesized materials is within the visible region i.e. 2.25 and 2.6eV for $CdIn_2S_4$ and $ZnIn_2S_4$ respectively. Therefore, activity of both the photocatalysts was tested for hydrogen generation by H_2S and H_2O splitting under natural solar light. The $ZnIn_2S_4$ photocatalyst is found to be more active for both H_2S and H_2O splitting reactions with H_2 evolution rate of $6994 \mu mol h^{-1} g^{-1}$ and $243 \mu mol g^{-1}$ respectively whereas for $CdIn_2S_4$ the rates are found to be $6128 \mu mol h^{-1} g^{-1}$ and $128.4 \mu mol g^{-1}$ respectively. The H_2 evolution rate by H_2S splitting was found to be much higher than the various reported nanostructured photocatalysts. The simple, environment friendly and cost effective method reported herein can be applicable for the large scale synthesis of XIn_2S_4 nanoparticles is the novelty of the present work.

1. Introduction

An important process for future energy supplies is hydrogen production from water and Hydrogen Sulfide. The photocatalytic splitting of H_2S and H_2O into hydrogen using solar light is a potentially clean and renewable source of energy. The cleavage of H_2S under visible light is of industrial importance, since H_2S occurs widely in natural gas fields and is produced in large quantities as an undesirable by-product in the coal and petroleum industry, mining, pulp and paper industry. Research on health, environment and air quality has long recognized that the release of sulfur compounds from refineries and flue stacks cannot go on unchecked. Hydrogen sulfide is a toxic and corrosive gas, exposure to H_2S causes a broad range of health problems when exposed to low concentrations and can be lethal when inhaled in large concentrations.¹

Currently, H_2S represents a negative-value commodity and using photocatalytic splitting it can be converted to useful

compounds by using solar energy which is highly desirable. The existing thermal-decomposition process for conversion of H_2S into sulphur is laborious and uneconomical. In this context, the photocatalytic splitting of H_2S into hydrogen has great technological importance. **Considering future requirement of zero emission fuel H_2 , has received fair attention from various research groups.** Although H_2 is produced industrially by various processes, photodecomposition of water into hydrogen generation has received immense importance. Considering the future importance of hydrogen as a fuel, recent photocatalysis research work has more focus on the photodecomposition of water and H_2S , to produce hydrogen under visible-light irradiation. Progress in photocatalysis in the past decade has been limited due to the use of UV light active photocatalysts instead of catalysts active under visible-light which is abundantly available.²⁻⁴ These catalysts operate with ultraviolet light, which accounts for only 4% of the incoming solar light reaching to earth surface and thus renders the overall process impractical. For the efficient utilization of solar radiation, a photo catalyst working in the visible region is of utmost importance, as the visible light constitutes around 45% of the solar radiation. The development of a visible-light photocatalyst has consequently become an imperative topic in

Centre for Materials for Electronics Technology, Panchavati, Off Pashan Road, Pune 411008 (M.S.) India. ^a-skapte@cmet.gov.in ^b-sonawane@cmet.gov.in – Corresponding authors

Electronic Supplementary Information (ESI) available: [details of any supplementary information available should be included here]. See DOI: 10.1039/x0xx00000x

current photocatalysis research. Recently, various types of visible-light-driven photocatalysts⁵⁻¹¹ for hydrogen generation have been reported. The stability and efficiency of some of the catalysts reported is still low and need improvement. In contrast to metal oxide photocatalysts, many metal sulfides have narrow band gap which corresponds to visible-light absorption.

Metal sulfides are known for their instability during the photocatalytic reaction, improvement in their stability is a great challenge to the use of CdS, for example, in the photoproduction of hydrogen¹². The problem of photo corrosion can be solved by incorporation of metal sulphides into the interlayer¹³. However, such stable catalysts showed very poor photocatalytic activity¹⁴. Cadmium Sulfide is a promising visible light active photocatalyst with a bandgap of 2.4 eV. But, it undergoes photo corrosion and efforts have been made to improve the stability of this catalyst.¹⁴

To overcome photo corrosion problem of CdS, many researcher synthesized $Cd_xZn_{1-x}S$ and studied their photocatalytic activities for H_2 evolution. Yanyan Li et al¹⁵ have synthesized twinned $Cd_xZn_{1-x}S$ solid solutions grown with several layers of defect-rich MoS_2 nanosheets and studied their photocatalytic activities for H_2 evolution from water splitting. Yanyan Li et al¹⁶ also conducted synthesis of solid-state Z-scheme photocatalyst $Cd_{1-x}Zn_xS@WO_{3-x}$. It consists of $Cd_{1-x}Zn_xS$ nanorods coated with oxygen-deficient WO_{3-x} amorphous layers and the synthesized photocatalyst was tested for H_2 evolution by water splitting. $Cd_{1-x}Zn_xS@WO_{3-x}$ was further hybridized by CoOx and NiOx nanoparticles through in-situ photo-deposition, by which the HER performance was further improved. Fangxu Dai et al¹⁷ reported the synthesis of magnetic $ZnFe_2O_4@ZnSe$ hollow nanospheres. In this work, higher photocatalytic activity has been achieved at optimal shell thickness of ZnSe.

The ternary sulfides have a strong absorption in the visible region hence they might be good candidates for the photo production of hydrogen¹⁸. It is reported that multicomponent metal sulfides and oxysulfides show better photocatalytic activity¹⁹ which implies that they could be a new class of photocatalyst. In the past few decades, although series of photocatalysts have been developed to improve photocatalytic activities for H_2 evolution, only a few effective visible-light-driven photocatalysts have been reported.²⁰⁻²² The ternary sulfides have attracted great attention as their properties can be facily adjusted by changing the composition to allow their versatile applications, such as in optical devices²³⁻²⁴ sensors²⁵ cathode materials²⁶ solar cell²⁷ and artificial photosynthesis.²⁸ Being applied as semiconductor photocatalysts, ternary sulfides have shown great promise in solar energy conversion because the band gap and redox levels of these metal sulfides can be controlled by adjusting the ratio of constituent elements, enabling the utilization of entire solar spectrum i.e. both UV and visible light. Recently, many ternary sulfides such as $AgIn_2S_4$, $Zn_{1-x}Cu_xS$ ²⁹⁻³² and $ZnIn_2S_4$ ³³ have been developed as photocatalysts. High quantum yield of 420% is reported when modified $AgInS_2$ is coupled with supportive water reduction catalysts.³⁴⁻³⁵ Cadmium Indium Sulfide ($CdIn_2S_4$) has been

regarded as a novel visible-light active photocatalyst for organic dye degradation³⁶⁻³⁸, photo production of hydrogen and bacterial inactivation.³⁹ Moreover, $CdIn_2S_4$ has received much attention due to it's potential applications in photoconductors, solar cells, optoelectronic devices and light emitting diodes (LEDs).⁴⁰ The first preparation of $CdIn_2S_4$ was reported by Hahn et al at 800°C under vacuum.⁴¹ One of the researchers⁴² also reported method for preparation of $CdIn_2S_4$ powders at high temperature using CdS and In_2S_3 as a precursors in the stoichiometric ratio of 1:2. Single crystals of $CdIn_2S_4$ were also grown from the stoichiometric elements by iodine-vapour transport⁴³⁻⁴⁴ or the horizontal Bridgman method.⁴² The preparation of one-dimensional (1D) nanostructures such as nanowires, nano rods and nanotubes is already a focus of the material world⁴⁵⁻⁵². As compared with micrometer-diameter whiskers, 1D structure is expected to have remarkable mechanical, electrical, optical, and magnetic properties. Existing technologies have been developed for the synthesis of some fascinating 1D inorganic materials.⁵²⁻⁵⁶ Ternary sulphides with various morphologies were prepared and reported by numerous scientists⁵⁷⁻⁶⁰. Recently, hydrothermal and solvothermal methods have been widely used to synthesize $CdIn_2S_4$ nanomaterials⁵⁷⁻⁶¹.

Resembling to $CdIn_2S_4$, $ZnIn_2S_4$ also has a suitable band gap corresponding to the visible-light absorption and excellent chemical stability for photocatalytic H_2 evolution⁶². It is the only semiconducting material with a layered structure in the AB_2X_4 family. It has attracted considerable attention because of its outstanding electrical and optical properties. Recently, various morphologies of $ZnIn_2S_4$ have been obtained by different methods using surfactants and have been used as a photocatalysts⁶³⁻⁶⁸. Batabyal et al⁶⁹ have synthesized In_2S_3 , $CdIn_2S_4$, and $ZnIn_2S_4$ nanocrystals and studied their photocatalytic activity for dye degradation under UV light. Recently Du et al⁶⁰ have synthesized monolayer and bilayer $ZnIn_2S_4$ and studied its photocatalytic performance for water splitting. Despite its good utility, very limited literature has been reported on these ternary materials although the synthesis of binary metal sulphides at large scale has been reported earlier.⁷⁰⁻⁷³ Therefore It is desirable to develop a simple, environment friendly, low-cost scalable method for the synthesis of nanostructured ternary metal sulphides viz. $CdIn_2S_4$ and $ZnIn_2S_4$. In view of this, a large-scale synthesis method to produce nanostructured $CdIn_2S_4$ and $ZnIn_2S_4$ is investigated herein. Here, the possibility of using a nano-material to facilitate splitting of H_2S into H_2 and molecular S through a chemical interaction, with a twofold goal: (i) elimination of the toxic gas from the environment and (ii) production of a clean energy fuel (H_2) with much lower heat of formation ($-4.77 \text{ kcal mol}^{-1}$) than H_2O ($-68.32 \text{ kcal mol}^{-1}$)⁷³.

In the present work, the large-scale synthesis of nanostructured ternary metal sulphides, XIn_2S_4 ($X=Cd, Zn$) from the bulk metal oxide precursors by a simple, template-free, low-temperature, solid-solid phase method is demonstrated. The proposed simple methodology is believed to be a significant breakthrough in the field of nanotechnology, and the method can be further generalized as a rational

preparation scheme for the large-scale synthesis, which will pave the way for commercialization.

2 Experimental sections

Chemicals : Analytical grade cadmium oxide, Zinc Oxide, Indium oxide and Thiourea were purchased from the local chemical manufacturer (Qualigens Fine Chemicals Pvt., Ltd., Mumbai, India) and were used as received.

2.1 Synthesis of XIn_2S_4

The XIn_2S_4 ($X = Cd, Zn$) nanostructures were prepared by solid state reaction. As received analytical reagent grade chemicals such as Cadmium Oxide (CdO), Zinc Oxide (ZnO), Indium Oxide (In_2O_3) and Thiourea (NH_2CSNH_2) were used without any purification. The stoichiometric amounts of $CdO/ZnO, In_2O_3, NH_2CSNH_2$ were taken in the molar ratio of 1:1:8 and mixed thoroughly using a pestle and mortar. The mixture was transferred to alumina crucible. The crucible is covered by keeping the lid and placed in an electric oven at $150^\circ C$ for 16, 20 and 24 hr respectively. The product obtained was washed thoroughly with distilled water to remove by-products if any and excess Thiourea followed by washing with anhydrous ethanol. The $CdIn_2S_4$ samples obtained are referred as CIS I, CIS II, CIS III and $ZnIn_2S_4$ samples are named as ZIS I, ZIS II, ZIS III respectively in the manuscript. The final product was dried at $70^\circ C$ for 4 h in a laboratory oven. Details of experiments carried out in the present study are summarized in table 1.

Table 1: Details of experimental conditions for the synthesis of XIn_2S_4

| Sr. No. | Sample Name | Sample ID | Temp. ($^\circ C$) | Duration (hrs) |
|---------|-------------|-----------|----------------------|----------------|
| 1 | $CdIn_2S_4$ | CIS I | 150 | 16 |
| 2 | | CIS II | | 20 |
| 3 | | CIS III | | 24 |
| 4 | $ZnIn_2S_4$ | ZIS I | 150 | 16 |
| 5 | | ZIS II | | 20 |
| 6 | | ZIS III | | 24 |

2.2.1 Optimization of precursor concentration for the preparation of phases pure XIn_2S_4 :

In order to optimize ratio of the precursors, particularly thiourea, initially the $CdIn_2S_4$ was prepared at similar conditions using theoretical ratio of 1:1:4 of $CdO:In_2O_3:NH_2CSNH_2$. The $CdIn_2S_4$ obtained using above ratio was analyzed by XRD for confirmation of the phase formation. The XRD results suggests that there is an incomplete formation of $CdIn_2S_4$ as presence of peaks corresponding to unreacted CdO, In_2O_3 are observed in XRD pattern. In addition to this, the yield of the product obtained was also far less than the theoretical yield. The above observation indicates that, the theoretical ratio of precursor is insufficient for the complete conversion of oxides into the respective Sulfides. From this study, it was confirmed that the precursor ratio, particularly thiourea is insufficient to produce phase pure $CdIn_2S_4$. The theoretical ratio i.e. 1:1:4, which leads to release insufficient sulfur molecules from H_2S produced during the reaction results in the incomplete formation of $CdIn_2S_4$. Therefore, the precursor ratio has been optimized by varying the concentration of Thiourea and accordingly Thiourea ratio for the synthesis of phase pure $CdIn_2S_4$ has been optimized. From the above study, it can be affirmed that the $CdO:In_2O_3:NH_2CSNH_2$ in the ratio of 1:1:8 is optimum for the formation of phase pure $CdIn_2S_4$ with fairly good

yield. In addition to the precursor ratio, the time and temperature of reaction has also been varied to optimize the reaction conditions. The time of reaction has been varied between to 12-24 hours and it is seen that the $CdIn_2S_4$ synthesized at lesser time duration shows the incomplete formation of $CdIn_2S_4$ with unreacted CdO and In_2O_3 phases. The XRD of $CdIn_2S_4$ samples obtained by variation of time are as shown in Supporting Information (figure S1). The XRD curve a corresponds to the sample prepared for 16 hrs and curve b is of the sample prepared for 12 hrs. The $CdIn_2S_4$ synthesized at lower reaction time does not show the complete phase formation as the peaks of individual reactants i.e. CdO and In_2O_3 are observed in XRD. This study confirms that, the optimum time required to achieve phase pure $CdIn_2S_4$ would be 16 hrs. The possibility of formation of individual phases of CdS or In_2S_3 is ruled out as the XRD spectra in Supporting information (figure S2) confirms the formation of phase pure $CdIn_2S_4$. In supporting information figure S2, XRD spectra of phase pure $CdIn_2S_4, CdS$ and In_2S_3 are given for comparison purpose. Similar study for optimization of precursor ratio, time duration and temperature of the reaction was also carried out for the preparation of phase pure $ZnIn_2S_4$ and the above optimized ratio of thiourea was used for the synthesis of $ZnIn_2S_4$. In this way all the reaction parameters have been fixed.

2.3 Photocatalytic study

2.3.1 Photocatalytic H_2 Evolution by H_2S Splitting

The photocatalyst was introduced as a suspension into a cylindrical quartz reactor. A Xe-lamp light source (LOT-Oriel Group, Europe, LSH302) of 450 W with cut off filter (> 420 nm) was used. At a constant temperature of $25 \pm 1^\circ C$, the vigorously stirred suspension was purged with argon for 1 h and then H_2S was bubbled through the solution for about 1 h. Each experiment was carried out using 0.5 g of catalyst in 750 mL of KOH solution (0.5 M) with a H_2S flow rate of 2.5 mL min^{-1} . The excess hydrogen sulfide was trapped in NaOH solution. The amount of hydrogen evolved was measured using a graduated burette and analyzed for its purity using gas chromatograph (Model Shimadzu GC-14B, Molecular Sieve 5Å column, with TCD and N_2 as carrier gas).

2.3.2 Photocatalytic H_2 Evolution from H_2O Splitting

In addition to H_2S splitting, photocatalytic activity of the prepared CIS and ZIS nanostructures was also investigated for photocatalytic water splitting. For this purpose 100 ml. double distilled water was taken in 250 mL round bottom flask, into this 25 mL methanol/ benzoyl alcohol was added as sacrificial reagent. The known quantity of prepared nanostructured photocatalyst was added to above solution along with 1 wt% Platinum as a co-catalyst. Argon gas was purged through this reaction mixture in order to remove the dissolved oxygen. The 250 mL round bottom flask was connected to the eudiometer tube to measure the evolved gas. The eudiometer tube has septum arrangement to remove the evolved gas through gas-tight syringe for quantifying the amount of gases evolved. The whole assembly kept in a wooden box containing reaction mixture was irradiated by 400W mercury vapor lamp. The mercury vapor lamp was fitted in quartz condenser having water circulation arrangement in order to absorb the IR radiation which minimizes the heating effect. As soon as the lamp switched on, the gas start evolving which is collected in eudiometer

tube. The amount of gas evolved with time were noted and used for the further calculations.

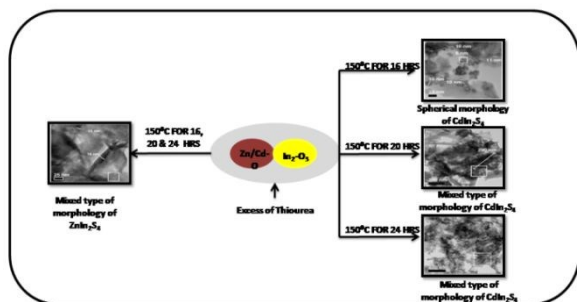
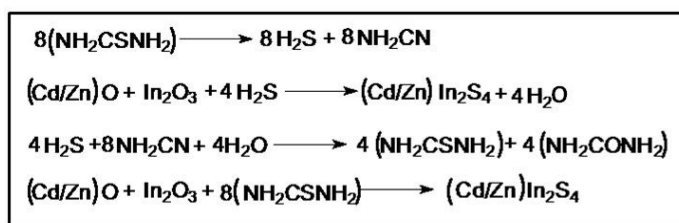
2.4 Samples Characterization

The as synthesized nanostructures were characterized by X-ray Diffractometry (Model-D8-Advance, Bruker AXS) for investigating its crystal phase. The samples were also characterized by TEM (Model JEM 2200 FS ,JEOL) to determine the particle size and morphology. XPS was carried out by using an ESCA-3000 instrument (VG Scientific Ltd., England). The BET technique was used to investigate the surface area on the model (Model Nova 1200 Series, Quantachrome, USA.). The optical properties were recorded using a UV/ visible–near-infrared (UV/Vis–NIR) spectrophotometer (PerkinElmer λ -950). Room temperature micro-Raman scattering (RS) was performed using a HR 800 Raman Spectrometer, (Horiba JobinYvon, France) with an excitation at 632.81 nm by a coherent He–Ne ion laser and a liquid nitrogen cooled CCD camera to collect and process the scattered data.

3 Results and Discussion

3.1 Formation Mechanism of $X\text{In}_2\text{S}_4$

The present solid-state method comprises a simple reaction between solids, namely Cadmium Oxide/Zinc Oxide, Indium



Scheme 1. Schematic representation for the formation of $X\text{In}_2\text{S}_4$

The formation of $X\text{In}_2\text{S}_4$ occurs via nucleation and crystal growth mechanism. At elevated temperature Thiourea decomposes and releases H_2S which acts as sulfur source. This H_2S slowly combines with $\text{Cd}^{2+}/\text{Zn}^{2+}$, In^{3+} ions and results in the formation of nuclei of $X\text{In}_2\text{S}_4$. The growth of these nuclei at saturated conditions leads to the formation of different morphological viz. spherical shaped nanorods and flake like nanostructures at higher time duration. Scheme 1 represents the schematic representation of formation of nanostructured $X\text{In}_2\text{S}_4$. Urea and thiourea are produced as a byproducts⁷¹ after completion of reaction and since both are water soluble, they can be easily separated from the respective sulphides viz CdIn_2S_4 and ZnIn_2S_4 . The prepared nanostructures were subjected for characterization using various instrumental techniques. The structural analysis was performed first to investigate the crystal structure.

3.2 Crystal Structure Study

3.2.1 X-Ray diffraction study of CdIn_2S_4 (CIS)

The crystal structure and phase purity of synthesized CdIn_2S_4 samples were investigated using powder X-ray diffraction (XRD) technique. Figure 1 shows XRD patterns of CdIn_2S_4 samples CIS I, CIS II, CIS III synthesized by solid state route at 150°C for durations of 16, 20 and 24 hours respectively. All the diffraction peaks are well matching with the reported JCPDS data (JCPDS File No. 270060) of Cubic spinel structure of CdIn_2S_4 ³⁶.

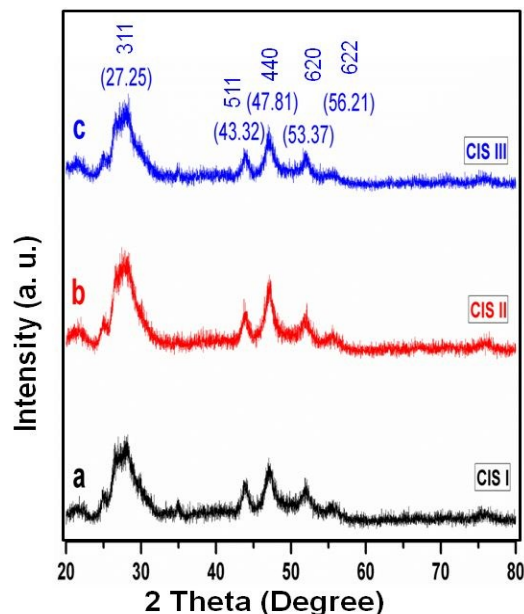


Fig. 1: XRD pattern of CdIn_2S_4 prepared at 150°C for (a) 16(b) 20 and (c) 24 hours

XRD pattern reveals that phase pure CdIn_2S_4 is formed as no separate peaks of individual CdS (JCPDS File No.10-0454) and In_2S_3 (JCPDS File No.05-0731) have been observed. The peaks in XRD pattern are broad in nature with high intensity peaks positioned at 2θ value at around 27° corresponding to 311 plane and peak at around 47.5° belongs to the 440 plane which are the main characteristic peaks of the cubic spinel structure of CdIn_2S_4 . The broad XRD pattern confirms the nanostructured nature of as synthesized CdIn_2S_4 . From the XRD data, the crystallite size of the CIS I, CIS II, CIS III samples were calculated using the Scherrer formula and it is found to be 8, 10, 15 nm respectively. From the calculation of crystallite size, it can be concluded that there is no significant effect of reaction time on crystallite size of as synthesized CIS. The crystallite size obtained closely matches with the particle size measured using HRTEM.

The slight increase in the crystallite size may be attributed to the growth of particles with time due to aggregation of particles. These results revealed that, a phase pure nanostructured CdIn_2S_4 with fairly good crystallinity can be synthesized at larger scale without addition of expensive reagents (surfactants/capping agents) via the present solid phase method.

3.2.2: X-Ray diffraction study of ZnIn_2S_4 (ZIS)

Synthesis of ZnIn_2S_4 using solid state route has been studied in a identical way and using same experimental conditions. **Figure 2** depicts the XRD patterns of the ZnIn_2S_4 samples synthesized via the solid phase method at different time intervals.

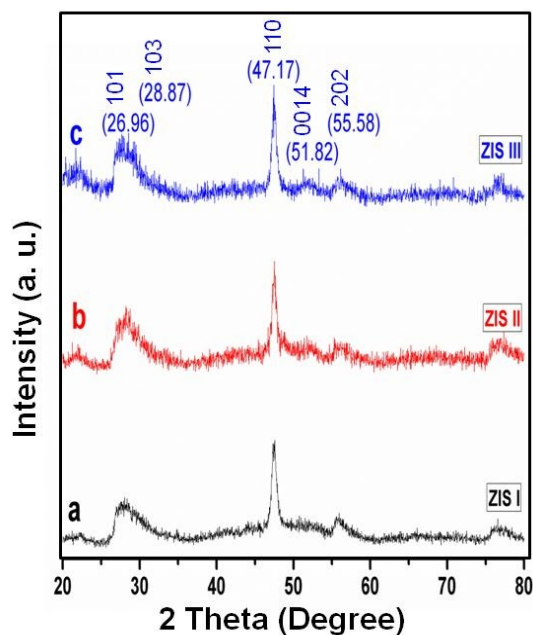


Fig. 2: XRD pattern of ZnIn_2S_4 prepared at 150°C for (a) 16 h (b) 20 h and (c) 24 hrs.

The XRD pattern confirms formation of hexagonal ZnIn_2S_4 as XRD data well matches with the hexagonal phase of ZnIn_2S_4 (JCPDS data No. 72-0773). The broad peaks in XRD patterns of all ZIS samples indicates that, as synthesized ZnIn_2S_4 is nanocrystalline in nature. The XRD peak at 2θ 26.96 (101) and 28.87° (103) are merged into single broad peak due to the nanocrystalline nature of as synthesized ZnIn_2S_4 . From the XRD data, the crystallite size of the ZIS I, ZIS II, ZIS III samples was calculated using the Scherrer formula and it is found to be 8, 13, 16 nm respectively. From the above study it is observed that, the closely analogous trend of particle growth has been observed for both the CIS and ZIS samples.

All the precursors used as well as CIS and ZIS synthesized herein have been analysed for its surface area using the Brunauer–Emmett–Teller (BET) technique. The results of surface area analysis are as tabulated in **table 2 and table 3**. Surface area of the precursor oxides showed negative isotherm suggesting that the precursors have low surface area

due to high crystallinity and coarse particle size. The specific surface area of the as synthesized CIS I, CIS II and CIS III samples found to be 46, 41, 38 m^2g^{-1} respectively. Similarly the specific surface area of ZIS I, ZIS II and ZIS III samples was found to be 45, 41 and 32 m^2g^{-1} respectively. The highest surface area was observed for the sample synthesized at 16 hours duration (for both CIS I and ZIS I). It has been observed that there is a decreasing trend of surface area of as synthesized XIn_2S_4 with increase in time duration of reaction has been observed and it may be due to increase in particle/crystallite size with duration of reaction.

Table 2: Structural, optical and photocatalytic properties of CdIn_2S_4 .

| Sample | Absorption Peaks (nm) | Band Gap (eV) as Calculated from Tauc Plot | Crystal Size (nm) from XRD | BET Surface area (m^2g^{-1}) | Rate of H_2 evolution ($\mu\text{mol h}^{-1}\text{g}^{-1}$) |
|---------|-----------------------|--|----------------------------|--|--|
| CIS I | 554 | 2.23 | 8 | 46 | 6128 |
| CIS II | 568 | 2.18 | 10 | 41 | 5440 |
| CIS III | 582 | 2.13 | 15 | 38 | 4423 |

3.3 Optical studies

3.3.1 Optical study of as synthesized CdIn_2S_4 (CIS)

The optical characterization of all as synthesized CdIn_2S_4 samples was performed using UV Vis DRS technique. The results obtained are as shown in Figure 3.

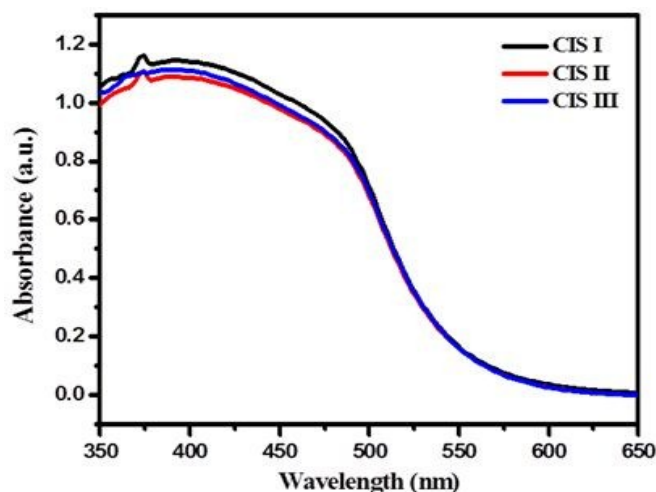


Fig. 3: UV-Vis spectra of as synthesized CdIn_2S_4 prepared at 150°C for (a) 16 h (b) 20 h and (c) 24 hrs

From the UV-VIS spectra (Figure 3), it is found that there is formation of single phase CdIn_2S_4 as no signs for presence of individual sulfides (CdS and In_2S_3) which is also confirmed by XRD. The single peak and steep absorption edge is supportive to above statement. The position of absorption peaks and corresponding band gap of as synthesized CdIn_2S_4 is tabulated in the Table 2. From the results, we can clearly see the red

shift in absorption edge for samples obtained by reaction of precursors for more duration. The CIS I, CIS II and CIS III samples show corresponding band gap of 2.23, 2.18, 2.13 eV respectively. This may be attributed to increase in crystallite size with time. As the size of CdIn_2S_4 increases, the corresponding band gap decreases which is in line with the expectations. Generally, it is observed that the band gap increases with time and temperature due to the growth of particles by agglomeration.

3.3.2 Optical study of as synthesized ZnIn_2S_4 (ZIS)

Figure 4 shows the UV-Vis spectra of as synthesized ZnIn_2S_4 samples. Similar to CdIn_2S_4 , ZnIn_2S_4 also shows identical optical behaviour.

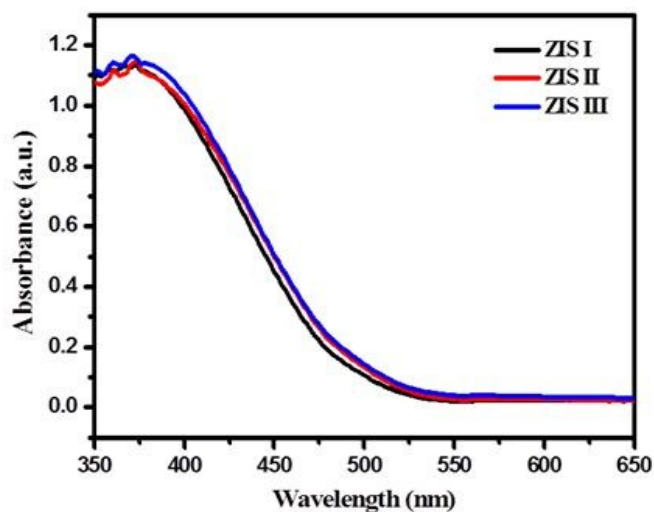


Fig. 4: UV-Vis spectra of as synthesized ZnIn_2S_4 prepared at 150°C for (a) 16, (b) 20 and (c) 24 hrs.

The single and steep absorption edge in the UV-Vis spectra suggest the formation of phase pure ZnIn_2S_4 . There is a red shift observed in the UV-Vis spectra of as synthesized ZnIn_2S_4 with increase in the reaction time. As discussed in earlier section this phenomenon is observed due to the increase in particle size of nanostructured ZnIn_2S_4 with time. The details of absorption edge and its corresponding band gap value are given in Table 3. Absence of peaks corresponding to individual ZnS and In_2S_3 phases suggest formation of phase pure ZnIn_2S_4 . The highest rate of H_2 generation of $6994 \mu\text{mol h}^{-1} \text{g}^{-1}$ was observed for ZIS I sample whereas lowest rate of H_2 generation was noted for ZIS III.

Table 3: Optical, structural and photocatalytic properties of ZnIn_2S_4 .

| Sample | Absorption Peaks (nm) | Band Gap (eV) as | Crystal Size (nm) from XRD | BET Surface area (m^2g^{-1}) | Rate of H_2 evolution ($\mu\text{mol h}^{-1} \text{g}^{-1}$) |
|---------|-----------------------|------------------|----------------------------|--|---|
| ZIS I | 470 | 2.63 | 8 | 45 | 6994 |
| ZIS II | 483 | 2.56 | 13 | 41 | 6541 |
| ZIS III | 492 | 2.52 | 16 | 32 | 6101 |

3.4 X-Ray Photoelectron Spectroscopy Study:

The surface characteristic, composition of both CdIn_2S_4 and ZnIn_2S_4 samples and ratio of Cd:In:S and Zn:In:S is obtained from the XPS analysis. The data obtained from analysis of both the samples is plotted and presented in Figure 5 and Figure 6 respectively. Figure 5 (a-d) shows the X-ray photoelectron spectroscopy (XPS) survey spectrum and the high-resolution Cd 3d, In 3d and S 2p spectra for the CdIn_2S_4 sample (CIS I) prepared by using $\text{CdO}:\text{In}_2\text{O}_3:\text{NH}_2\text{CSNH}_2$ at molar ratio of 1:1:8 respectively. The sample CIS I is chosen as a representative sample because it shows high BET Surface area and highest H_2 generation rate. The binding energies obtained were corrected for specimen charging by referencing carbon 1s to 284.5 eV. The survey spectrum shows the peaks corresponding to Cd3d, S 2p and In3d elements.

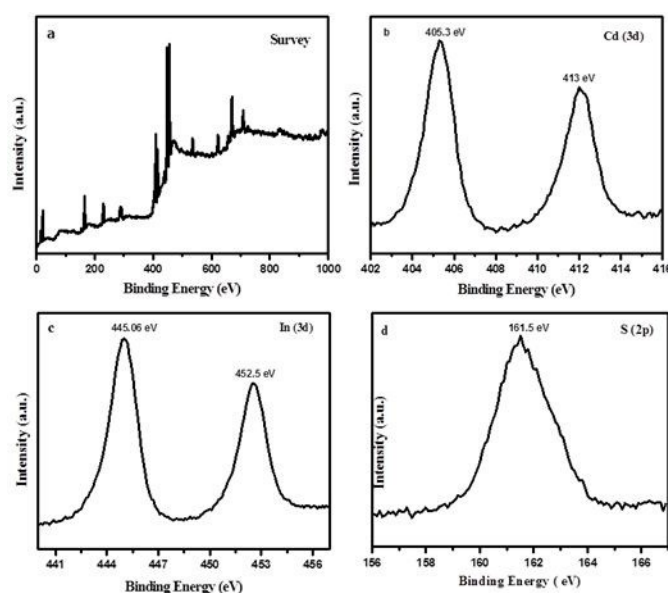


Fig. 5: XPS spectra of CIS-I (a) Survey spectra (b) Cd(C) In (d)S

The Oxygen peak is mostly due to the adsorbed moisture on the surface of CIS sample. Otherwise the spectrum is clean with absence of peaks for C and N from the reactants. The single S 2p peak at 161.5eV is indicative of sulfur present as the S^{2-} , whereas the two sharp peaks in Figure 5b at 404.6 and 411.41eV are attributed to the 3d level of Cd atoms. The Cd 3d and S 2p3 peaks at binding energies 205.3 (Cd 3d5), 413 (Cd 3d3) and 161.5eV (S 2p3) were attributed to the CdS molecular environment. The peaks are in good agreement with data reported in the literature. Two peaks at 445.06, 452.5eV as seen in fig 5c pertaining to In 3d and these peaks are

corresponding to $3d_{5/2}$ and $3d_{3/2}$ spin-orbit spin components only. The area under the curve has been measured and used for calculating the elemental ratio of all the elements present in the nano-crystals. The XPS results show Cd:In:S ratio of 1:1.89:3.93 which is very close to and in good agreement with the theoretical values.

The surface characterization of the ZnIn_2S_4 sample (ZIS I) is as shown in Figure 6 (a-d). The survey spectrum shown in figure 6a shows the presence of peaks corresponding to Zn, In and S only. The careful observation of Figure 6 b shows the peak at 1026 eV and 1049 eV corresponding to Zn 2p levels. The Indium peaks at 449.2 and 456.7 eV in Fig 6c are corresponding to the existence of In 3d states. However, the peak at 165.5 eV in fig 6d due to presence of S 2p states into the sample. Indium and Sulfur peaks are observed at 444.2 eV ($\text{In}3d_{5/2}$) 165.5 eV ($\text{S}2p_{3/2}$) respectively.

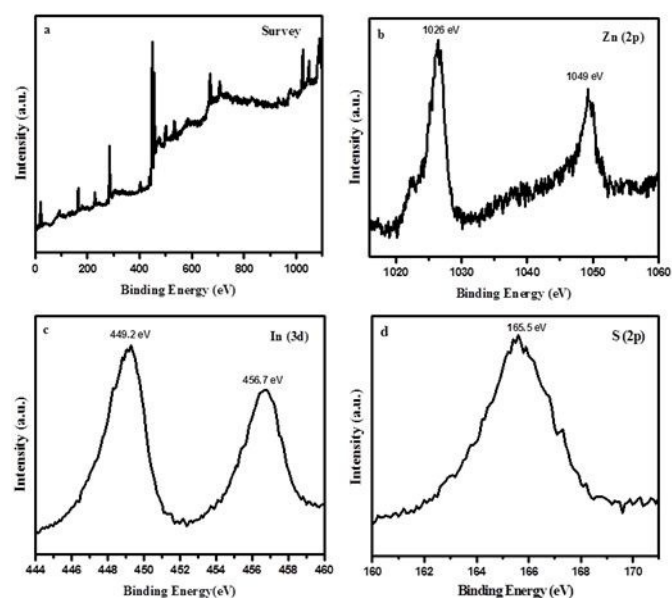


Fig. 6: XPS spectra of ZIS-I (a) Survey spectra, (b) Zn, (c) In and (d) S

This implies the existence of elements In^{3+} , S^{2-} and Zn^{2+} chemical states into the sample. The area under the curves of these peaks is utilized for the calculation of the molar % of Zn, In and S present in ZnIn_2S_4 . The observed molar ratio of the representative ZIS I sample is 1 : 1.99 : 4 (Zn:In:S) which is very close to the theoretical value. No other peaks pertaining to any trace impurities were observed indicating absence of such impurities into the ZnIn_2S_4 sample. The XPS analysis confirms the stoichiometry of ZIS samples and it can be seen that the compositions of ZIS is very close to the theoretical composition.¹⁴

3.5 Raman Study:

In order to confirm the formation of CdIn_2S_4 and ZnIn_2S_4 phases the representative samples (CIS I and ZIS I) were analyzed using Raman Spectroscopy. Figure 7 a and b represents the Raman Spectra of CIS I and ZIS I respectively.

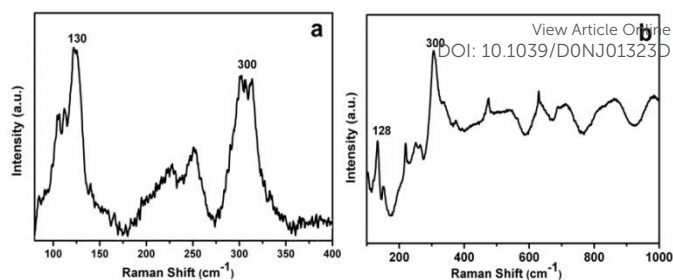


Fig. 7: Room temperature Raman spectra of (a) CIS I and (b) ZIS I

Intense and sharp peak at 130 cm^{-1} and broad peak at around 300 cm^{-1} are attributed to the cubic spinel CdIn_2S_4 .⁷⁴ In Raman spectrum of CIS and ZIS, it is seen that there are no peaks of individual CdS and In_2S_3 which itself supports complete conversion of precursor to phase pure cubic spinel CdIn_2S_4 . Raman spectra of ZIS I sample is as shown in figure 7 b and it confirms the formation of phase pure ZnIn_2S_4 . The distinguished peaks at 128 and 300 cm^{-1} are corresponding to the hexagonal spinel ZnIn_2S_4 .⁷⁵ The results of UV-Vis, Raman and XRD analysis are complementary to each other and are well matching with previously reported data^{14, 38, 74, 75}.

3.6 Surface and morphological studies

The size and morphology of as synthesized CdIn_2S_4 and ZnIn_2S_4 have been investigated using HRTEM analysis.

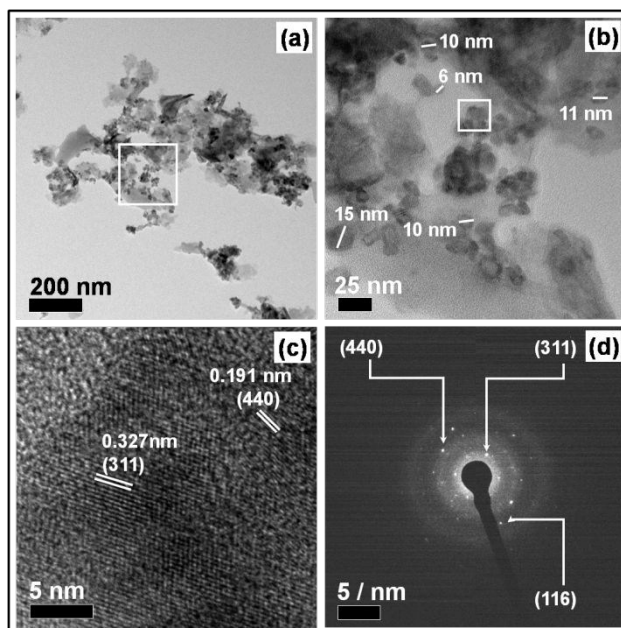


Fig.8: HRTEM images of CIS I (a) low magnification, (b) high magnification, (c) Lattice image and (d) ED pattern

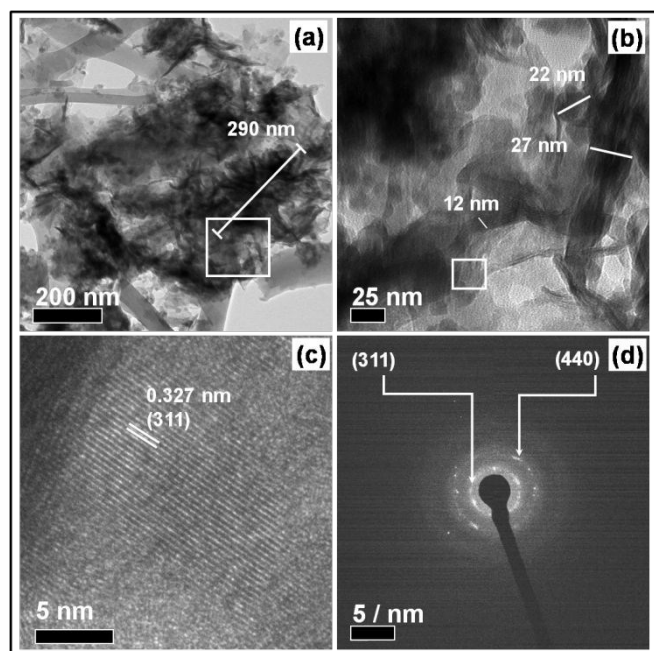


Fig.9: HRTEM images of CIS II (a) low magnification, (b) high magnification, (c) Lattice image and (d) ED pattern.

Figure 8, 9 and 10 represents the TEM images of CIS I, CIS II and CIS III samples respectively. In HRTEM image, CIS I sample shows the formation of spherical and rod like mixed morphological particles. The careful observation of image indicates that, the average particle sizes of spherical particles are in the range of 10 nm and rods are having average diameter of 30 nm. In case of CIS II (Fig. 9) and CIS III (Fig.10) samples, no appreciable difference in morphology has been observed even though the reaction time was extended.

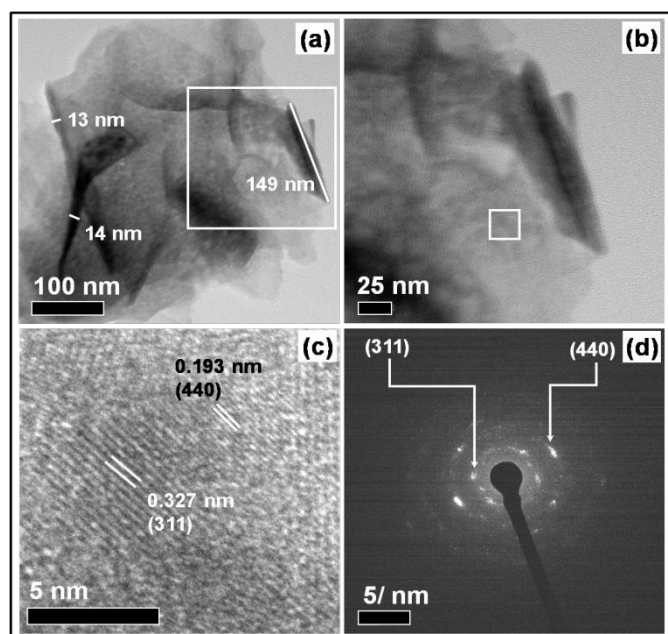


Fig.10: HRTEM images of CIS III (a) low magnification, (b) high magnification, (c) Lattice image and (d) ED pattern.

However, in CIS II and CIS III samples, the particles are seen to be more define and separated with spherical particles of size 10-15 nm and rod of diameter 30-40 nm. The images figure 8 c, 9 c and 10 c gives information about crystal orientation and d spacing values of CdIn_2S_4 crystals.

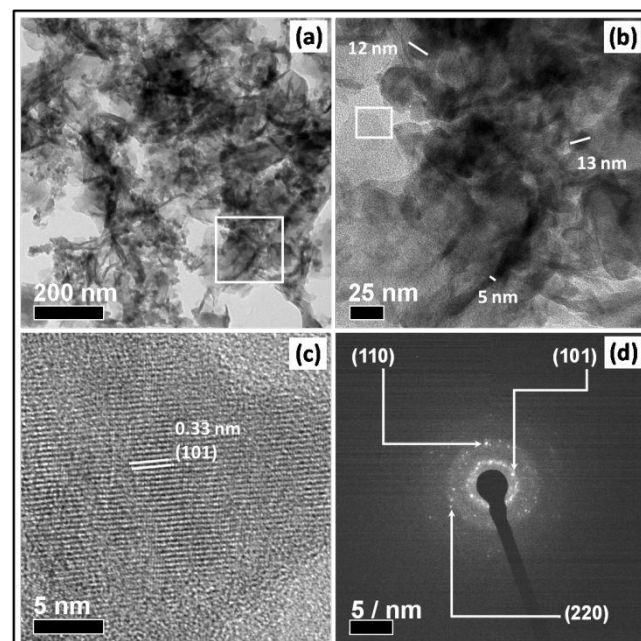


Fig.11: HRTEM images of ZIS I (a) low magnification, (b) high magnification, (c) Lattice image and (d) ED pattern.

The d spacing values of **0.327 nm** and **0.191 nm** obtained from lattice image are in good agreement with the theoretical values and the predominant orientation of crystals is in **311** directions. The spot type Electron diffraction (ED) pattern shows the formation of single crystalline CdIn_2S_4 with fairly good crystallinity. Compositional analysis of CdIn_2S_4 was carried out using EDAX technique. Results of the EDS analysis are given in **table S1** Supporting Information. The EDAX analysis performed at various spots also confirms the composition of CdIn_2S_4 which is very close to theoretical composition. Figures 11, 12 and 13 depict the HRTEM images of ZnIn_2S_4 , ZIS I, ZIS II and ZIS III samples respectively. In case of ZIS I (Fig. 11a) very thin flake like structure with thickness of more than 13 nm and length of 140 nm onwards.

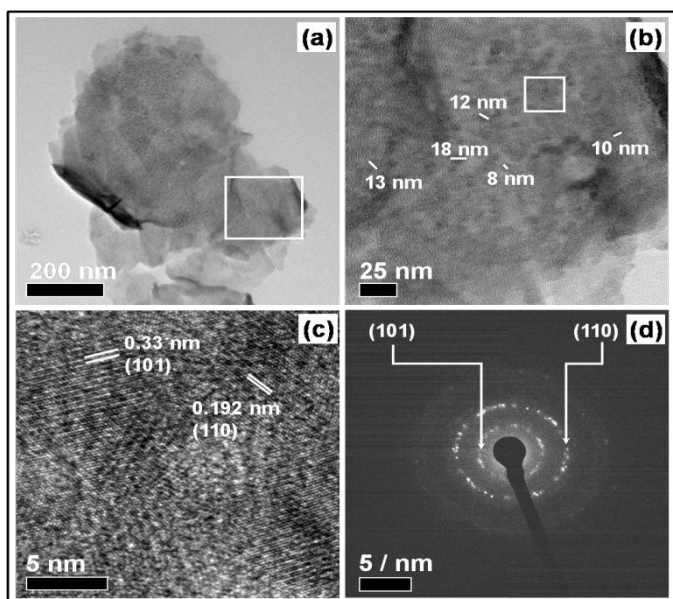


Fig. 12: HRTEM images of ZIS II (a) low magnification, (b) high magnification, (c) Lattice image and (d) ED pattern.

Figure 11c shows a high resolution image of selected area (square marked) in the Fig 11b depicts the lattice fringes of **0.33** and **0.192** nm associated with the 101 and 110 plane of hexagonal ZnIn_2S_4 . The spot type electron diffraction pattern in figure 11d confirms the formation of single crystalline hexagonal ZnIn_2S_4 with good crystallinity.

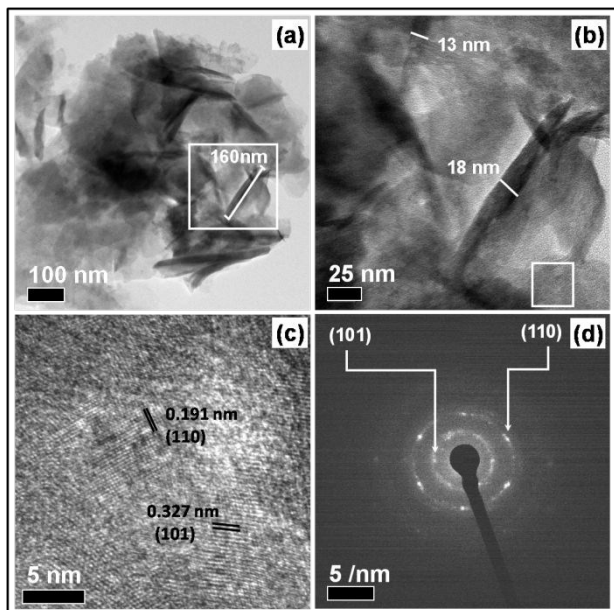


Fig. 13: HRTEM images of ZIS III (a) low magnification, (b) high magnification, (c) Lattice image and (d) ED pattern.

In case of ZIS II and ZIS III samples no significant difference in morphology and structure has been observed. However as per the data given in Table 3, the particle size is seen to be increasing with reaction time. In case of ZIS II (Figure 12 a, b) the flakes are seen to become more significant. The ED

pattern Figure 12d confirms hexagonal structure which is well in agreement with the results obtained by XRD. In case of ZIS III (Figure 13 a, b) well defined, flake like structure is observed with diffused pattern which may be attributed to the longer reaction time and increased particle size.

4. Photocatalytic Study

4.1 Photocatalytic Activity Measurements:

The as synthesized CdIn_2S_4 and ZnIn_2S_4 shows the band gap in range of 2.63-2.13eV, hence the photo catalytic activity of the samples has been investigated under visible light irradiation. The photo activity of both the photocatalyst was tested for splitting the H_2S and H_2O under visible light irradiation. The experimental set up used for the study of photocatalytic activity is described in the experimental section.

4.2 Photocatalytic H_2 evolution from H_2S Splitting:

The CdIn_2S_4 samples were tested for its photocatalytic activity by splitting of H_2S under visible light irradiation. The plot of amount of H_2 evolution with time by photo splitting of H_2S is as shown in Figure 14. The result shows that photocatalytic activity decreases with reaction time for synthesis of CdIn_2S_4 . The CIS I prepared at lower time duration shows the highest rate of H_2 evolution as compared with CIS II and CIS III samples. This may be due to the lower particle size of CdIn_2S_4 and highest surface area at lower time duration. The CIS I sample shows H_2 evolution at the rate of $6128 \mu\text{mole h}^{-1} \text{g}^{-1}$ whereas CIS II and CIS III samples show H_2 evolution at the rate of 5440 and $4423 \mu\text{mole h}^{-1} \text{g}^{-1}$, respectively. The decrease in the rate of H_2 evolution of CIS II and CIS III samples may attribute to the increase in the particle size and subsequent decrease in surface area of CdIn_2S_4 .

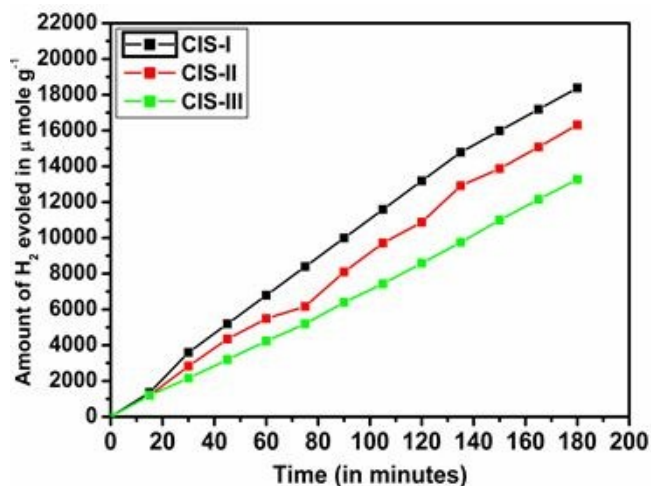


Fig. 14: Time conversion plots of H_2 evolution by splitting H_2S using CdIn_2S_4 photocatalyst.

Similarly, the photocatalytic activity of ZnIn_2S_4 samples for H_2 evolution using H_2S was carried out under visible light irradiation. Unlike CdIn_2S_4 a similar trend of results for H_2 generation has been observed. The ZIS I sample shows the highest rate of H_2 evolution i. e. $6994 \mu\text{mole h}^{-1} \text{g}^{-1}$ whereas ZIS II and ZIS III show the H_2 evolution at the rate of 6541 and $6101 \mu\text{mole h}^{-1} \text{g}^{-1}$ respectively. Here also the results obtained

are much higher than the earlier reported photocatalyst bulk CdS⁷². It is well known that the photocatalysts comprising of P-block metal ion (In^{3+}) with d10 configuration are known to possess good photocatalytic activities for water decomposition^{14, 38}. As synthesized CdIn_2S_4 and ZnIn_2S_4 contains In^{3+} ions in the d10 configuration. Therefore, we strongly feel that this could be one of the reasons for achieving good photocatalytic activity for as synthesized CdIn_2S_4 and ZnIn_2S_4 .

As the crystal structure of CdIn_2S_4 ³⁸, the distance of Cd and S (2.52 eV) is shorter than that of In and S (2.62 eV), it shows that circuitously, we tried to stabilize CdS. In this case, the conduction bands are composed of mainly 5S orbital of cadmium atoms mixing with small amount of 5d orbital of indium atoms. This composed conduction band is responsible for obtaining good photocatalytic activity.

In this case, as synthesized ZnIn_2S_4 shows good photocatalytic activity because of the layered hexagonal structure. In the hexagonal structure of ZnIn_2S_4 , the atoms are arranged in layers at six equally separated levels along the c-axis. Each of the Zn^{+2} ions are in a tetrahedral environment of four S atoms; In^{+3} ions are in two environments, an octahedral environment of six S atoms and a tetrahedral environment of four S atoms.¹⁴ This layered structure is responsible for the good photocatalytic activity for ZnIn_2S_4 .

The obtained results of H_2 evolution from H_2S splitting are compared with previously reported data. In previous studies, CdIn_2S_4 and ZnIn_2S_4 were synthesized by clumsy conventional methods like hydrothermal or solvothermal synthesis. The details of rate of H_2 evolution of previously reported CdIn_2S_4 and ZnIn_2S_4 are given in table S2 in supporting information. From the Table S2, it can be revealed that the rate of H_2 evolution of previously reported CdIn_2S_4 and ZnIn_2S_4 is slightly higher than present work^{12, 14, 38, 76}. As mentioned earlier, previously reported CdIn_2S_4 and ZnIn_2S_4 were synthesized by conventional methods like hydrothermal or solvothermal method, the possibility of controlling the particle size and morphology is high owing to obtain narrowly distributed nano particles with uniform morphology. Due to the uniform morphology, and narrow sized distribution of CdIn_2S_4 and ZnIn_2S_4 nanoparticles, these researchers reported higher photocatalytic activity. But, the earlier reported methods have number of limitations viz. 1) requires expensive precursors 2) require different types of surfactants / capping agents to avoid particle agglomeration 3) very less product is obtained after reaction, so difficult to scale up the process for large scale synthesis. However, the method used in the present work (solid phase) has many advantages as compared to hydrothermal / solvothermal methods. As mentioned above the present work describes the large-scale synthesis of nanostructured tertiary XIn_2S_4 (X=Cd, Zn) from the bulk metal oxide precursor by a simple, template free, low-temperature, solid-solid phase method. Besides this, better practical yield of the product can be obtained via present method. Therefore, we feel that slightly lower rate of H_2 evolution obtained in the present work using CdIn_2S_4 and ZnIn_2S_4 as compared with reported work^{12, 14, 38, 76} is reasonably acceptable.

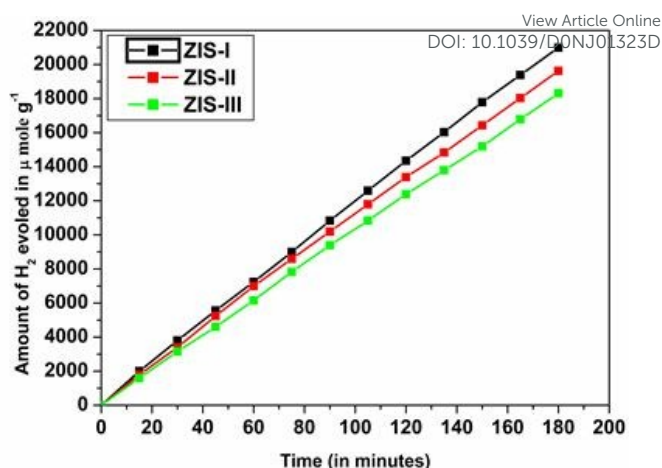


Fig. 15: Time conversion plots of H_2 evolution by splitting H_2S using ZnIn_2S_4 photocatalyst.

The stability of both the photocatalysts i. e. CdIn_2S_4 and ZnIn_2S_4 was tested by reusing the photocatalyst for more than one time. The photocatalyst recovered from previous experiment was dried and reused again for next experiment.

Table 4: Photocatalytic performance of CdIn_2S_4 and ZnIn_2S_4 photocatalyst after reuse.

| Sr. No. | Sample | Rate of H_2 evolution ($\mu\text{mol h}^{-1} \text{g}^{-1}$) | Rate of H_2 evolution ($\mu\text{mol h}^{-1} \text{g}^{-1}$)- Reused |
|---------|---------|---|---|
| 1 | CIS I | 6128 | 6085 |
| 2 | CIS II | 5440 | 5390 |
| 3 | CIS III | 4423 | 4376 |
| 4 | ZIS I | 6994 | 6912 |
| 5 | ZIS II | 6541 | 6502 |
| 6 | ZIS III | 6101 | 6098 |

The details of the results of photocatalytic activity of both the photocatalyst reused are given Table 2. From the results, it is seen that there is slight deactivation of catalysts when it is used for the second time. However, the deactivation is very less which suggests that both the photocatalysts are quite stable as compared with CdS hence it can be used for number of times without noticeable deactivation. No substantial degradation of both the photocatalysts has been seen after the photocatalytic activity, which is also confirmed from XRD analysis. XRD spectra of reused CdIn_2S_4 and ZnIn_2S_4 samples are given in the supporting Information (figure S3).

4.3 Photocatalytic H_2 evolution from H_2O Splitting

The as synthesized sample of CdIn_2S_4 and ZnIn_2S_4 were tested for the photocatalytic activity of H_2 generation from photo splitting of H_2O under visible light irradiation. The results of photocatalytic activity for H_2 generation by H_2O splitting of both photocatalyst are shown in Figure 16. The organic alcohols such as methanol and benzoyl alcohol have been used as hole scavengers. The results of H_2O splitting using above hole scavenger shows that CIS I produces $114.3 \mu\text{mol g}^{-1}$ of

H₂ within four hours of irradiation using methanol as hole scavenger where as under identical reaction condition it showed 135.7 $\mu\text{mol g}^{-1}$ of H₂ in similar time duration using benzyl alcohol as sacrificial reagent.

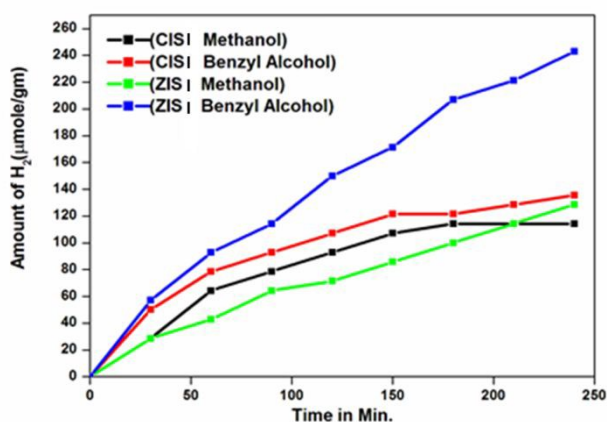


Fig. 16: Time conversion plots of H₂ evolution by splitting H₂O using CdIn₂S₄ and ZnIn₂S₄ photocatalyst.

Similarly, the ZIS I produced 128.4 $\mu\text{mol g}^{-1}$ of H₂ in presence of methanol in 4 hr but under identical conditions using benzoyl alcohol as scavenger, it produces H₂ of 243 $\mu\text{mol g}^{-1}$ within same duration. The results suggests that the ZnIn₂S₄ is showing better activity for H₂O splitting and almost double the amount of H₂ produced using benzoyl alcohol as compared to methanol. More the activity of photocatalyst by using benzoyl alcohol may be attributed to fast oxidation of benzoyl alcohol by capturing holes and better separation of electron and holes in this process ultimately results in more activity. This consecutively produced higher amount H₂ as compared to methanol and other scavengers. We have also compared the obtained results of the rate of H₂ evolution for H₂O splitting with previously reported data of rate of H₂ evolution using CdIn₂S₄ and ZnIn₂S₄ photocatalysts. Table S3 in supporting information gives the details of comparison data of rate of H₂ evolution with other similar photocatalysts. From the table S3, it is concluded that as synthesized CdIn₂S₄ and ZnIn₂S₄ shows the slightly lower rate of H₂ evolution from H₂O as compared to reported work⁷⁷⁻⁸¹. The justification for slightly lower rate of H₂ evolution is already given in previous section.

Conclusions

Herein, we report the large scale synthesis of XIn₂S₄ by simple, environmental friendly and cost effective solid phase method. The XRD analysis of as synthesized samples shows the formation of phase pure compound of CdIn₂S₄ and ZnIn₂S₄. The size of CdIn₂S₄ prepared at 150°C for 16, 20 and 24 hours duration shows the crystallite size of 8, 10, 15 nm respectively. Whereas, ZnIn₂S₄ synthesized at 150°C for 16, 20 and 24 hours show the crystallite size of 8, 13, 16 nm respectively. The BET surface area analysis of CdIn₂S₄ and ZnIn₂S₄ shows high surface area as compared to their precursors which implies the nanostructure nature of as synthesized CdIn₂S₄ and ZnIn₂S₄ sample. The HRTEM images of CdIn₂S₄ shows spherical and rod

like mixed morphology with particle size of 8-15 nm for spherical particles and 30-40 nm for rods. Also, ZnIn₂S₄ shows the mix type of morphology of spherical (10-27 nm) and flakes like structure with thickness of around 13 nm and length of around 140 nm. The band gap estimation shows the values for CdIn₂S₄ and ZnIn₂S₄ in the range of 2.23-2.13 eV and 2.63-2.52eV respectively. Photocatalytic study of the both photocatalysts shows an excellent photocatalytic activity for H₂ generation by splitting of H₂S and H₂O under visible light irradiation. The obtained results of photocatalytic activity are much higher than the earlier reported photocatalysts. Additionally, both the photocatalysts show excellent stability and reproducibility for reuse on number of occasions.

Conflicts of interest

In accordance with our policy on [Conflicts of interest](#) please ensure that a conflicts of interest statement is included in your manuscript here. Please note that this statement is required for all submitted manuscripts. If no conflicts exist, please state that "There are no conflicts to declare".

Acknowledgements

The authors would like to thank Dr. K. R. Patil and Ms. Rupali P. Waichal, Scientists NCL, Pune, India for providing XPS and Raman Spectra. Help from Dr. N C Pramanik, Scientist, C-MET, Trissur for the BET measurements is also acknowledged. The authors also would like to thank the Ministry of Electronics & Information Technology (MeitY), New Delhi, India, for financial support.

References

- J. Lindenmann, V. Matzi, N. Neuboeck, B. Ratzenhofer-Komenda, A. Maier and F.-M. Smolle-Juettner, *Diving Hyperb. Med.*, 2010, **40**, 213–217.
- A. Fujishima, K. Honda, *Nature*, 1972, **37**, 138.
- S. V. Tambvekar, M. Subrahmanyam, *Int. J. Hydrogen Energy* 1997, **22**, 959.
- A. Mills, S. L. Hunte, *J. Photochem. Photobiol., A*, 1997, **108**, 1
- C. A. Linkous, N. Z. Muradov, S. N. Ramser, *Int. J. Hydrogen Energy* 1995, **20**, 701.
- Z. Zou, H. Arakawa, *J. Photochem. Photobiol., A* 2003, **158**, 145-.
- B. B. Kale, J. O. Baeg, J. S. Yoo, S. M. Lee, C. W. Lee, S. J. Moon, H. Chang, *Can. J. Chem.* 2005, **83**, 527-.
- H. G. Kim, D. W. Hwang, J. S. Lee, *J. Am. Chem. Soc.* 2004, **126**, 8912-.
- I. Tsuji, H. Kato, H. Kobayashi, A. Kudo, *J. Am. Chem. Soc.* 2004, **126**, 13 406.
- A. Ishikawa, T. Takata, J. N. Kondo, M. Hara, H. Kobayashi, K. Domen, *J. Am. Chem. Soc.* 2002, **124**, 13 553-.
- M. Liu, W. You, Z. Lei, G. Zhou, J. Yang, G. Wu, G. Ma, G. Luan, T. Takata, M. Hara, K. Domen, C. Li, *Chem. Commun.* 1998, **357**, 4–10]
- Bharat B. Kale, Jin-OokBaeg, Sang Mi Lee, Hyunju Chang, Sang-Jin Moon, and Chul Wee Lee, *Adv. Funct. Mater.* 2006, **16**, 1349–1354.

- 13 W. Shangguan and A. Yoshida, *J. Phys. Chem. B*, 2002, **106**, 12227.
- 14 Nilima S. Chaudhari, Ashwini P. Bhirud, Ravindra S. Sonawane, Latesh K. Nikam, Sambhaji S. Warule, Vilas H. Rane and Bharat B. Kale *Green Chem.*, 2011, **13**, 2500.
- 15 Yanyan Li, Bowen Sun, Haifeng Lin, Qinqin Ruan, Yanling Geng, Jie Liu, Hui Wang, Yu Yang, Lei Wang, Kam Chiu Tam, *Applied Catalysis B: Environmental*, 2020, **267**, 118702.
- 16 Yanyan Li, Qinqin Ruan, Haifeng Lin, Yanling Geng, Jiefei Wang, Hui Wang, Yu Yang and Lei Wang, *Sci China Mater*, 2020, **63**, 75.
- 17 Fangxu Dai, Ruiyang Zhao, Xudong Huai, Jishu Han, Lei Wang, Shouhua Feng, *Composites Part B: Engineering*, 2019 **173**, 106891
- 18 R Sasikala, A R. Shirole, V. Sudarsan, K G Girija, Rekha Rao, Chandran Sudakar and S R Bharadwaj, *J. Mater. Chem.*, 2011, **21**, 16566.
- 19 D. Park, J. O. Beag, *US Patent 6 297 190 B1*, **2001**, D. Park, J. O. Beag, *US Patent 6 447 650 B1*, **2002**
- 20 Fujishima A, Honda K. *Nature*, 1972, **238**, 7.
- 21 Fox MA, Dulay MT. *Heterogeneous photocatalysis. Chem Rev.*, 1993, **93**, 341-357.
- 22 Kato H, Asakura K, Kudo A. *J. Am. Chem. Soc.*, 2003, **125**, 3082.
- 23 J. Feng, M. Sun, F. Yang and X. R. Yang, *Chem. Commun.*, 2011, **47**, 6422.
- 24 L. Tian, H. I. Elim, W. Ji and J. J. Vittal, *Chem. Commun.*, 2006, 4276.
- 25 J. C. Yu, J. Zhang and S. W. Liu, *J. Phys. Chem. C*, 2010, **114**, 13642-
- 26 R. Kanno and M. Maruyama, *J. Electrochem. Soc.*, 2001, **148**, A742.
- 27 B. D. Weil, S. T. Connor and Y. Cui, *J. Am. Chem. Soc.*, 2010, **132**, 6642.
- 28 T. Arai, S. Tajima, S. Sato, K. Uemura, T. Morikawa and T. Kajino, *Chem. Commun.*, 2011, **47**, 12664.
- 29 A. Kudo and M. Sekizawa, *Catal. Lett.*, 1999, **58**, 241.
- 30 J. G. Yu, J. Zhang and M. Jaroniec, *Green Chem.*, 2010, **12**, 1611-
- 31 Y. Wang, J. C. Wu, J. W. Zheng and R. Xu, *Catal. Sci. Technol.*, 2011, **1**, 940
- 32 Y. Wang, J. C. Wu, J. W. Zheng, R. R. Jiang and R. Xu, *Catal. Sci. Technol.*, 2012, **2**, 581.
- 33 Z. X. Chen, D. Z. Li, W. J. Zhang, Y. Shao, T. W. Chen, M. Sun and X. Z. Fu, *J. Phys. Chem. C*, 2009, **113**, 4433.
- 34 I. Tsuji, H. Kato, H. Kobayashi and A. Kudo, *J. Am. Chem. Soc.*, 2004, **126**, 13406.
- 35 T. Torimoto, T. Adachi, K. Okazaki, M. Sakurakawa, T. Shibayama, B. Ohtani, A. Kudo and S. Kuwabata, *J. Am. Chem. Soc.*, 2007, **129**, 12388.
- 36 S. K. Apte, S. N. Garaje, R. D. Bolade, J. D. Ambekar, M. V. Kulkarni, S. D. Naik, S. W. Gosavi, J. O. Baeg, B. B. Kale, *J. Mater. Chem.* 2010, **20**, 6095.
- 37 J. Mu, Q. Wei, P. Yao, X. Zhao, S. Kang, X. Li, *J. Alloys Compd.* 2012, **513**, 506.
- 38 A. Bhirud, N. Chaudhari, L. Nikam, R. Sonawane, K. Patil, J. Baeg, B. Kale, *Inter. J. hydrogen energy* 2011, **36**, 11628.
- 39 W. Wang, T. W. Ng, W. K. Ho, J. Huang, S. Liang, T. An, G. Li, J. C. Yu, P. K. Wong, *Appl. Catal. B: Environ.* 2013, **129**, 482.
- 40 R. R. Sawant, K. Y. Rajpure, C. H. Bhosale, *Phys. B*, 2007, **393**, 249
- 41 Hahn, H., Frank, G., Klinger W., Stoerger A. and Stoerger S. Z., *Anorg. Allg. Chem.*, 1955, **279**, 241.
- 42 Kerimova T. G., Salaev E. Y., Khidirov A. S., Dervishov N. G., and Efendiev S. H., *Phys. Stat. Sol. B* 1982, **113**, K107.
- 43 Charlebois, A. and Fortin, E., *J. Appl. Phys.* 1989, **66**, 3220.
- 44 Charbonneau S. Fortin and E. Beauvais, *J. Can. J. Phys.* 1987, **65**, 204.
- 45 Rao A. M., Richter E., Bandow S., Chase B., Eklund, P. C., William K. A., Fang, S., Subbaswamy K. R., Menon, M. Thess A., Smalley R. E. Dressehaus, G. Dressehaus, M. S. *Science*, 1997, **275**, 187.
- 46 Bockrath, M., Cobden D. H., McEuen P. L., Chopra N. G., Zettl A., Thess A., Smalley R. E., *Science* 1997, **275**, 1922.
- 47 Suenaga K., Colliex C., Demoncey N., Loiseau A., Pascard H., Willaime F., *Science* 1997, **278**, 653.
- 48 Jirage K. B., Hulteen J. C., Martin, C. R., *Science*, 1997, **278**, 655.
- 49 Chopra N. G., Luyken R. J., Cherrey K., Crespi V. H., Cohen M. L., Louie S. G., Zettl, A., *Science*, 1995, **269**, 966.
- 50 Saito, S. *Science*, 1997, **278**, 77.
- 51 Collins, P. G.; Zettl, A.; Bando, H.; Thess, A.; Smalley, R. E. *Science*, 1997, **278**, 100.
- 52 Morales, A. M. Lieber, C. M. *Science* 1998, **279**, 208-
- 53 Iijima, S. *Nature* 1991, **354**, 56
- 54 Dai, H., Wong, E. W., Lu Y. Z., Fan, S. and Lieber C. M. *Nature* 1995, **375**, 769.
- 55 Trentler, T. J.; Hickman, K. M.; Goel, S. C.; Viano, A. M.; Gibbons, P. C.; Buhro and W. E. *Science* 1995, **270**, 1971.
- 56 Pan Z., Lai H. L., Au F. C. K., Duan X., Zhou W., Shi W., Wang N., Lee C. S., Wong N. B., Lee S. T., and Xie S., *Adv. Mater.* 2000, **12**, 1186.
- 57 Lu J, Xie Y, Du G, Jiang X C, Zhu L Y and Wang X Y, *Mater Chem.*, 2002, **12**, 103.
- 58 Fan L and Guo R. *J. Phys. Chem. C* 2008, **112**, 10700.
- 59 Mu J, Wei Q L, Yao P P, Zhao X L, Kang S Z, Li X Q. *J Alloys Compd.*, 2012, **512**, 506.
- 60 Li YX, Dillert R, Bahnemann D. *Thin Solid Films* 2008, **516**, 4988.
- 61 Peng SJ, Mhaisalkar SG and Ramakrishna S. *Mater Lett.* 2012; **79**, 216.
- 62 Yaoguang Yu, Gang Chen, Gang Wang, Zushun Lv., *Inter. Jou. Of Hydro. En.* 2013, **3**, 8, 1278.
- 63 Z. B. Lie, W. S. You, M. Y. Liu, G. H. Zhou, T. Takata, M. Hara, K. Li and C. Domen, *Chem Commun.*, 2003, 2142.
- 64 X. L. Gou, F. Y. Cheng, Y. H. Shi, L. Zhang, S. J. Peng, P. W. Chen and J. Shen, *J. Am. Chem. Soc.*, 2006, **128**, 7222.
- 65 X. L. Hu, J. C. Yu, J. M. Gong and Q. Li, *Cryst. Growth Des.*, 2007, **7**, 2444.
- 66 Z. Chen, D. Li, W. Zhang, C. Chen, W. Li, M. Sun, Y. He and X. Fu, *Inorg. Chem.*, 2008, **47**, 9766.
- 67 F. Fang, L. Chen, Y. B. Chen and L. M. Wu, *J. Phys. Chem. C*, 2010, **114**, 2393.
- 68 S. Shen, L. Zao and L. Guo, *Int. J. Hydrogen Energy*, 2008, **33**, 4501- Z. Lei and W. You, *Chem. Commun.*, 2003, 2142.
- 69 Sudip K. Batabyal, Shu En Lu, and Jagadese J. Vittal, *Cryst. Growth Des.*, 2016, **16**, 2231.
- 70 S. N. Garaje, S. K. Apte, S. D. Naik, J. D. Ambekar, R. S. Sonawane, M. V. Kulkarni, Ajayan Vinu, and B. B. Kale, *Environ. Sci. Technol.* 2013, **47**, 6664.
- 71 S. K. Apte, S. N. Garaje, G. P. Mane, Ajayan Vinu, S. D. Naik, D. P. Amalnerkar and B. B. Kale, *Small* 2011, **7**, 957.
- 72 S. K. Apte, S. N. Garaje, S. S. Arbuj, B. B. Kale, Jin O. Baeg U. P. Mulik, S. D. Naik, D. P. Amalnerkar and S. W. Gosavi, *J. Mater. Chem.*, 2011, **21**, 19241.
- 73 Summayya Kouser, Umesh V. Waghmare and Nacir Tit, *Phys. Chem. Chem. Phys.*, 2014, **16**, 10719.
- 74 J. Q. Hu, B. Deng, W. X. Zhang, K. B. Tang, and Y. T. Qian, *Inorg. Chem.*, 2001, **40**, 3130.
- 75 S. Shen, L. Zhao, X. Guan and L. Guo, *Journal of Physics and Chemistry of Solids*, 2012, **73**, 79.
- 76 N. S. Chaudhari, S. S. Warule and B. B. Kale, *RSC Advances*, 2014, **4**, 12182.
- 77 A. Meng, B. Zhu, B. Zhong, L. Zhang, B. Cheng, *Appl. Surf. Sci.*, 2017, **422**, 518.

Journal Name

ARTICLE

- 78 M. A. Mahadadalkar, S. B. Kale, R. S. Kalubarme, A. P. Bhirud, J. D. Ambekar, S. W. Gosavi, M. V. Kulkarni, C. J. Park, B. B. Kale, *RSC Adv.*, 2016, **6**, 34724.
- 79 M. A. Mahadadalkar, S. W. Gosavi, and B. B. Kale, *J. Mater. Chem. A*, 2018, **6**, 16064.
- 80 C. Dua, Q. Zhangb, Z. Lina, B. Yana, C. Xiab and G. Yanga, *Applied Catalysis B: Environmental*, 2019, **248**, 193.
- 81 J. Shen, J. Zai, Y. Yuan, X. Qian, *Inter. J. hydrogen energy*, 2012, **37**, 16986.

View Article Online
DOI: 10.1039/D0NJ01323D

1
2
3
4
5
6
7
8
9
10
11
12
13
14
15
16
17
18
19
20
21
22
23
24
25
26
27
28
29
30
31
32
33
34
35
36
37
38
39
40
41
42
43
44
45
46
47
48
49
50
51
52
53
54
55
56
57
58
59
60

Facile Template Free Approach for the Large Scale Solid Phase Synthesis of Nanocrystalline XIn_2S_4 (X=Cd/Zn) and it's Photocatalytic Performance for H_2 Evolution.

View Article Online
DOI: 10.1039/C4ONJ01323D

Sonali D. Naik, Sanjay K. Apte,^{*a} Sunil N. Garaje, Yogesh A. Sethi, Manish D. Shinde, Sudhir A. Arbuji, Bharat B. Kale and Ravindra S. Sonawane^{*b}

Centre for Materials for Electronics Technology, Panchavati, Off Pashan Road, Pune 411008 (M.S.) India. ^{*a}- skapte@cmet.gov.in ^{*b}- sonawane@cmet.gov.in – Corresponding authors

Nanostructured $CdIn_2S_4$ and $ZnIn_2S_4$ with unique morphology can be synthesized using this method which is simple and easy to operate.

